# Monitoring Light Source for CMS Lead Tungstate Crystal Calorimeter at LHC

Liyuan Y. Zhang, Kejun J. Zhu, Ren-Yuan Zhu, and Duncan T. Liu

*Abstract*—Light monitoring will serve as an intercalibration for compact muon solenoid (CMS) lead tungstate crystals *in situ* at the large hadronic collider, which is crucial for maintaining crystal calorimeter's subpercent constant term in the energy resolution. This paper presents the design of the CMS electromagnetic calorimeter monitoring light source and high-level distribution system. The correlations between variations of the light output and the transmittance for the CMS choice of yttrium-doped PbWO$_4$ crystals were investigated and were used to study monitoring linearity and sensitivity as a function of wavelength. The monitoring wavelength was determined so that a good linearity as well as adequate sensitivity can be achieved. The performance of a custom manufactured tunable laser system is presented. Issues related to monitoring precision are discussed.

*Index Terms*—Calibration, crystal, laser, monitoring, radiation damage.

## I. INTRODUCTION

**B**ECAUSE of its high density and fast decay time, lead tungstate (PbWO$_4$) crystal was chosen by the compact muon solenoid (CMS) experiment to construct a precision electromagnetic calorimeter (ECAL) at the large hadronic collider (LHC). In the last five years, an extensive research and development (R&D) program has been carried out to develop radiation hard PbWO$_4$ crystals. As a result of this development program, a total of 11.2 m$^3$ large size (25 X$_0$) yttrium-doped PbWO$_4$ crystals with fast light output will be produced in the Bogoroditsk Techno-Chemical Plant (BTCP) in Tulla, Russia, and the Shanghai Institute of Ceramics (SIC) in Shanghai, China. The crystals, however, still suffer from nonnegligible radiation damage [1]–[7]. Our previous studies concluded that the scintillation mechanism in PbWO$_4$ is not affected by radiation, and the loss of the light output is due only to the absorption caused by radiation-induced color centers [7]. The variations of transmittance can be used to predict variations of the light output. A light monitoring system, which measures variations of the transmittance, thus may provide crucial intercalibration *in situ* at LHC, making a precision calorimeter possible even by using PbWO$_4$ crystals that suffer from radiation damage [8].

In this paper, we report the design of the CMS monitoring light source and high-level distribution system. A monitoring test bench was carried out to study correlations between variations of the light output and the transmittance for the CMS choice of Y-doped PbWO$_4$ crystals. The monitoring linearity and sensitivity as a function of wavelength were investigated and were used to determine the monitoring wavelength so that the best linearity and an adequate sensitivity are achieved. The performance of a custom manufactured tunable laser system in a 135-h long-term stability test is presented. Issues related to monitoring precision are discussed.

## II. DESIGN OF MONITORING LIGHT SOURCE AND HIGH-LEVEL DISTRIBUTION SYSTEM

A precise calibration *in situ* is a key in maintaining the precision offered by a crystal calorimeter. For the CMS PbWO$_4$ calorimeter, frequent intercalibration *in situ* at LHC is provided by a light monitoring system, which injects light pulses into each individual crystal and measures variations of its optical transmission and uses that to predict variations of its light output. The monitoring light pulses produced by a laser system are distributed via an optical fiber system organized into three levels [9]: a fiber-optic switch that sends laser pulses to one of 80 calorimeter elements (72 half super modules in the barrel and eight groups of super crystals in two endcaps) and a two level distribution system mounted on each calorimeter element, which delivers monitoring pulses to each individual crystal. Combined with physics events, such as electron pairs from the Z$^0$ decays and single electrons from the W decays, the monitoring system is expected to provide calibrations with a precision of 0.4%.

Fig. 1 is a schematic showing the design of the monitoring light source and high-level distribution (optical switch). The laser system is required to be able to produce light pulses at two wavelengths [9]. As discussed in our previous report, the choice of monitoring wavelength directly affects the monitoring sensitivity and linearity [8]. To track down variations of crystal light output caused by radiation damage and recovery *in situ*, the monitoring system must run 100% time during the data taking. To provide a continuous monitoring *in situ*, a fraction of the 3.17-$\mu$s beam gap in every 88.924-$\mu$s LHC beam cycle [10] will be used to inject monitoring light pulse into crystals. Our initial requirements for the laser light source are as follows [11].

1)  Two wavelengths: one close to the emission peak that provides the best monitoring linearity for the CMS choice of Y-doped crystals and the other providing a cross check:
2)  *spectral contamination:* $<10^{-3}$;
3)  *pulse width:* full-width at half-maximum (FWHM) $<40$ ns to match the ECAL readout;
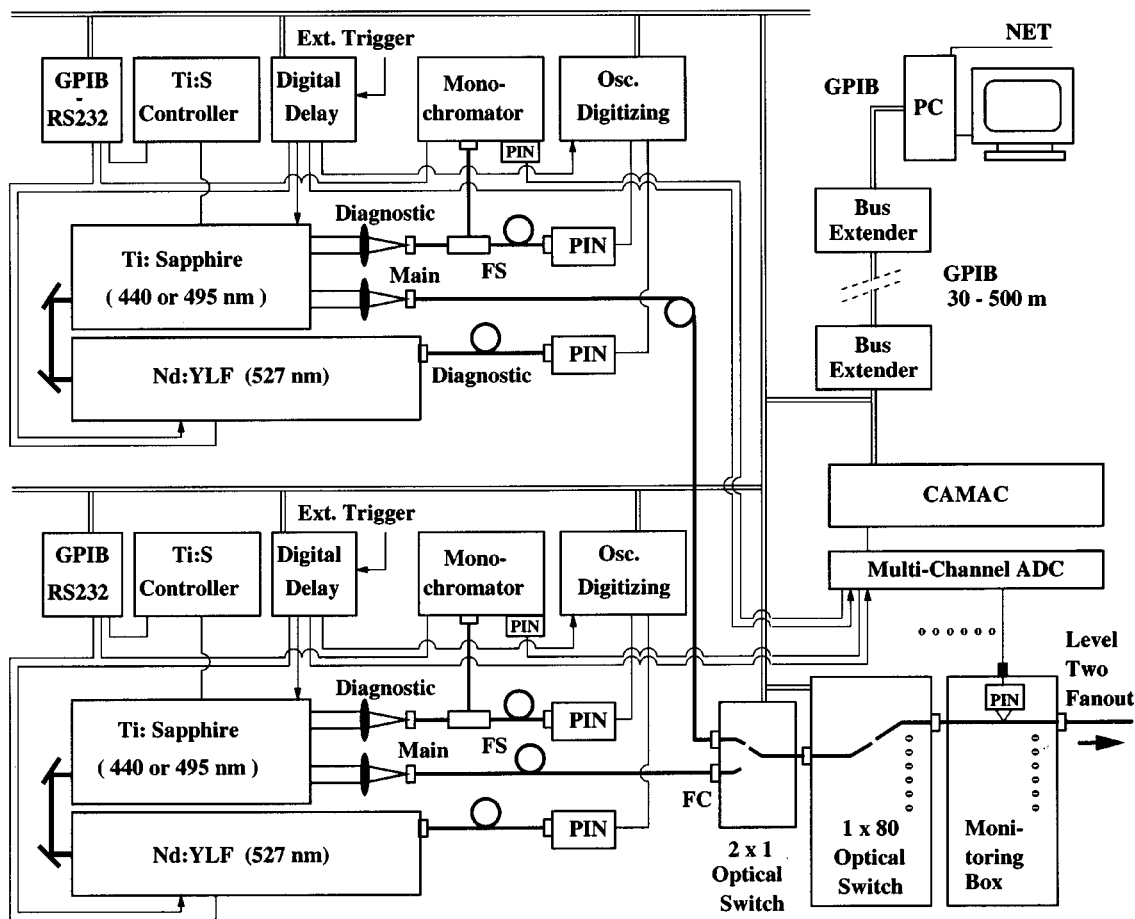
Fig. 1.   The conceptual design of the monitoring light source and high-level distribution system for the CMS PbWO$_4$ calorimeter.

4) *pulse jitter:* <3 ns for trigger synchronization to the LHC beam;

5) *pulse rate:* ~80 Hz, which is the maximum rate allowed by the ECAL data-acquisition system;

6) *pulse energy:* 1 mJ/pulse at monitoring wavelength, which provides a dynamic range up to 1.3 TeV in a single crystal;
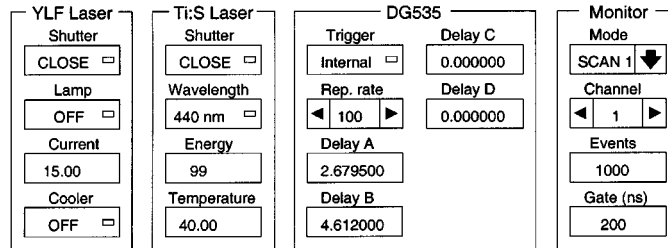
7) *pulse-to-pulse instability:* <10%.

Our design of the light source consists of two sets of lasers, each consisting of an Nd:YLF pump laser and a tunable Ti:Sapphire laser. Two sets of lasers are necessary to guarantee 100% availability of the monitoring system. The controls of the entire system—such as internal/external trigger mode, repetition rate and delay times, Nd:YLF laser shutter status, lamp status, pump current and cooler status, Ti:Sapphire laser shutter status, wavelength choice, energy level, and cooling temperature—are set by a central computer through GPIB and RS-232 interfaces. Fig. 2 shows the laser setting control window.

Each set of lasers has a main output and a diagnostic output. The diagnostic output is further split into two fibers by using a fiber splitter. One output goes to a monochromator for wavelength spectrum monitoring, as shown in Fig. 3. The other goes to a digital scope for pulse shape and timing monitoring, as shown in Fig. 4. The pulse shape recorded by digital scope is analyzed by a computer. The histograms and history of laser pulse



Fig. 2.   The setting window showing control parameters for an Nd:YLF pumping laser, a Ti:S laser, and the run control.

energy, FWHM, jitter, and wavelength spectra obtained by the monochromator and the digital scope are stored in the computer.

The selection of two main outputs is controlled by a 2 × 1 fiber-optic switch. The output of this 2 × 1 switch is distributed via a 1 × 80 fiber-optic switch to 80 calorimeter elements through 150-m-long quartz fibers. Before sending laser pulses to the level-2 splitters, a monitoring box is used to measure pulse energies in each channel. The history of pulse energy passing each switch channel is also stored in the computer.

## III. CHOICE OF MONITORING WAVELENGTH

Fig. 5 is a schematic showing a monitoring test bench used at the California Institute of Technology (Caltech)to investigate
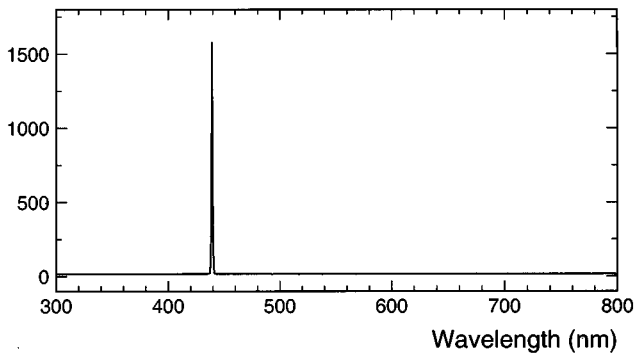
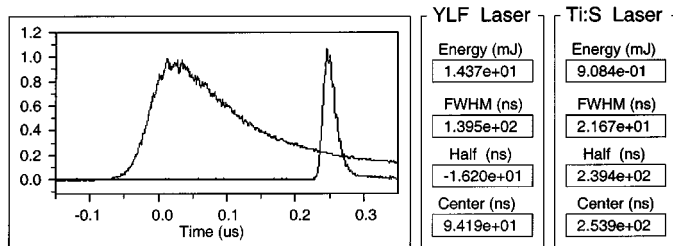Fig. 3.    The wavelength display showing wavelength spectrum.

Fig. 4.    The laser pulse shape display showing a wide pulse from the YLF:Nd pumping laser, a narrow pulse from the Ti:S laser, and performance of two lasers.
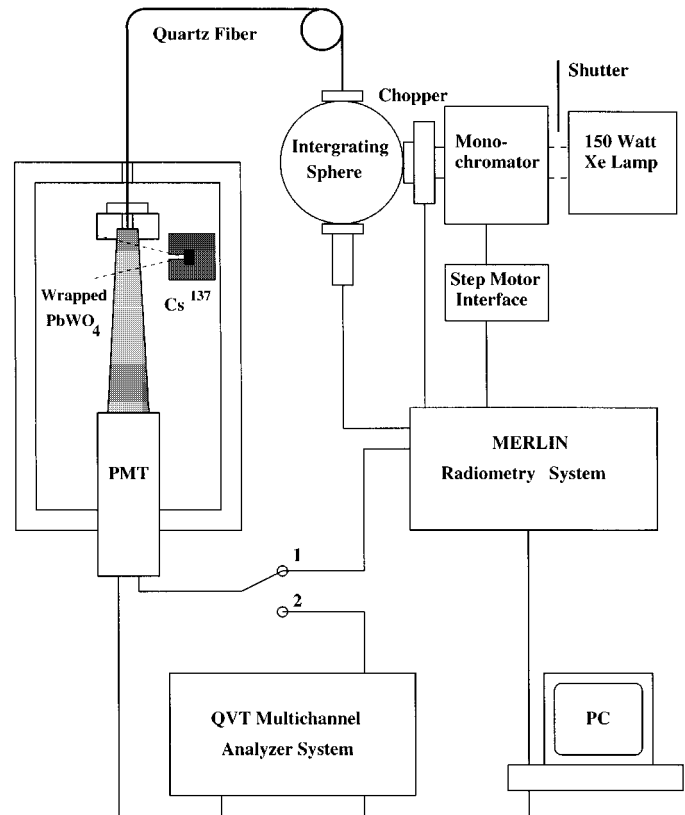
Fig. 5.    The monitoring test bench for the transmittance (position 1) and light output (position 2) measurement.

Fig. 6.    Distribution of the PMT output normalized to the reference detector on the sphere (position 1 in Fig. 5), taken in 23 h.

monitoring sensitivity and linearity. The monitoring light from a xenon lamp went through a monochromator and was injected to an integrating sphere. The light from one output of the sphere was coupled to the front end of a sample through a quartz fiber and an air gap. The light from the other output of the sphere was measured by a photodetector as a reference. The sample was wrapped with two layers of Tyvek paper and was optically coupled to a PMT. The output of the PMT is coupled to either a Merlin from ORIEL through a lock-in amplifier for the transmittance measurement (position 1) or a LeCroy QVT multichannel analyzer for the light output measurement (position 2).

When the switch is in position 1, the transmittance as a function of wavelength was measured by using the PMT output normalized to that of the reference detector. The reference detector was thermoelectrically cooled to reduce systematic uncertainties caused by fluctuations of the intensity of the light source. The PMT output was chopped and went through a lock-in amplifier to suppress the noise. Fig. 6 shows a distribution of the PMT output normalized to the reference detector taken for a sample in 23 h. A Gaussian fit shows that the stability of the transmittance measurement, defined as $\sigma/\mu$ (width/average) of the fit, to be better than 0.1%.

When the switch is in position 2, the shutter at the input of the monochromator is closed so that there is no interference of the monitoring light source. The scintillation light output of the sample was measured by using a small $^{137}$Cs source and a LeCroy 3001 QVT in the $Q$ mode. The Cs spectrum was fit to a simple Gaussian to determine the peak position, which then was converted to the light output in pe/MeV by using a calibration of the single photoelectron peak. Fig. 7(a) shows 20 measurements of the light output taken in 9 h for a sample coupled to a PMT. Data were corrected by using the room temperature,
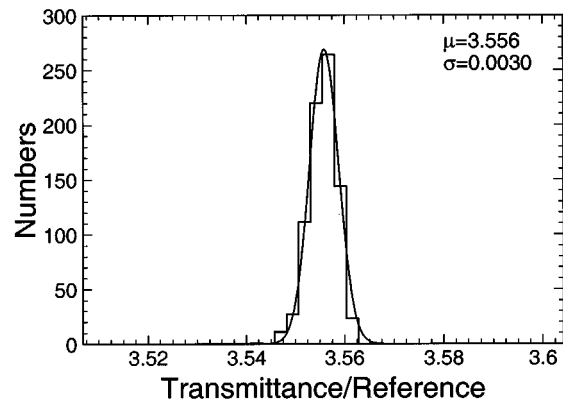
which has a variation of up to 0.5 °C, despite central air conditioning of the entire laboratory building and individual temperature adjustment and feedback in each room. Fig. 7(b) and (c) shows raw and temperature-corrected light outputs, respectively, and the corresponding Gaussian fit. A precision of 0.8 and 0.6% was achieved for the light output measurement without and with temperature corrections, respectively.

To simulate expected radiation environment *in situ* at LHC, samples were either irradiated by a $^{60}$Co source under 15–1000 rad/h or under recovery after the irradiation. Fig. 8 shows correlations between the relative variations of transmittance ($\Delta T/T$) and the relative variation of the light output ($\Delta LY/LY$) for the monitoring light at four different wavelengths—(a) 410, (b) 440,
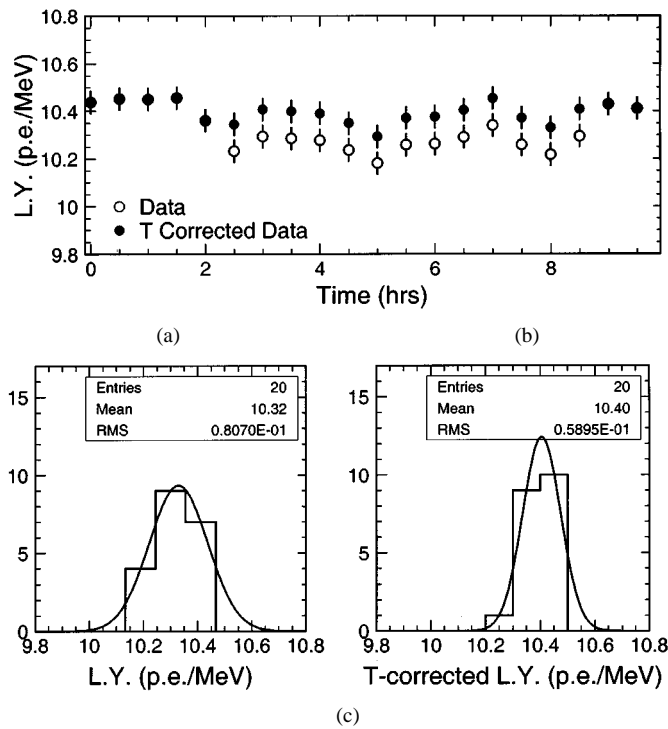
Fig. 7. (a) Light output measured by the PMT through a LeCroy QVT (position 2 in Fig. 5), taken in 9 h, and its distributions (b) without and (c) with temperature corrections.
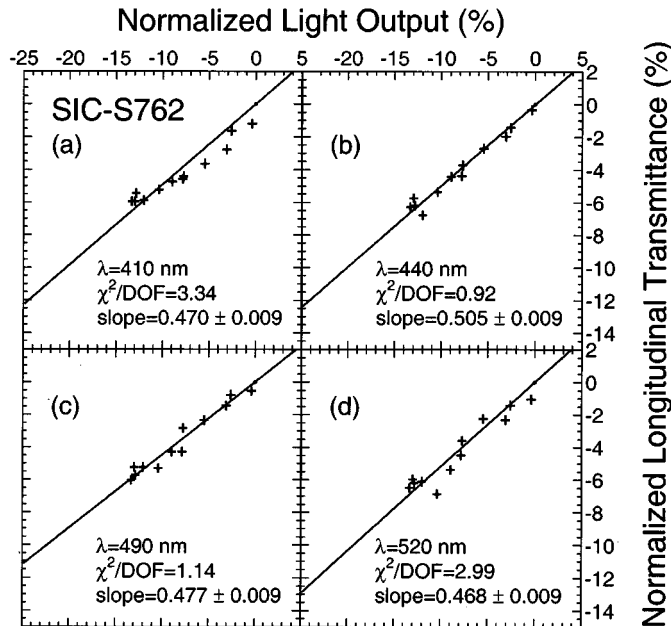


Fig. 8. Correlations between relative variations of transmittance and light output are shown at monitoring wavelengths of (a) 410, (b) 440, (c) 490, and (d) 520 nm for a Y-doped sample SIC-S762.

(c) 490, and (d) 520 nm—for a Y-doped sample SIC-S762. The correlation was fit to a linear function

$$\frac{\Delta T}{T} = \text{slope} \times \frac{\Delta LY}{LY} \qquad (1)$$

The result of the fit, including the $\chi^2$/DoF and the slope, is also shown in the figure for each monitoring wavelength. The error
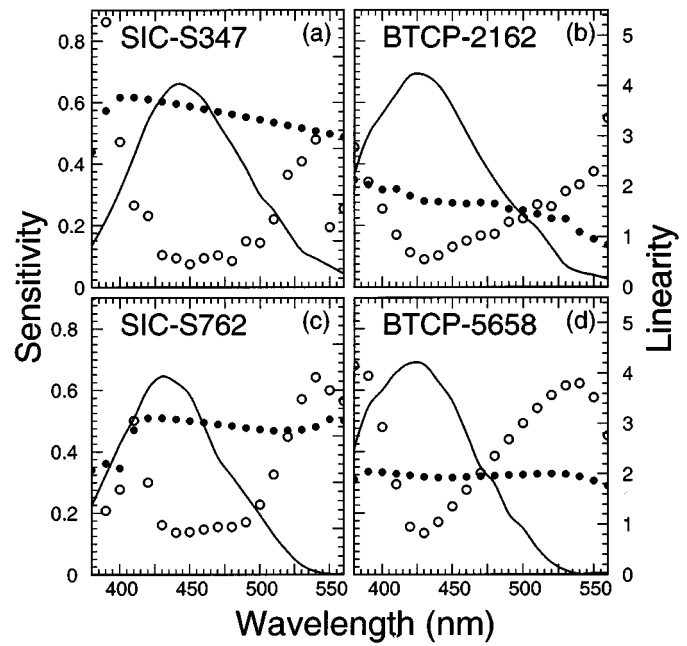


Fig. 9. Monitoring sensitivity (solid dots), linearity (open dots), and emission spectrum (solid lines) are shown as functions of wavelength for samples (a) SIC-S347, (b) BTCP-2162, (c) SIC-S762, and (d) BTCP-5658.

on the slope is about 2–3%, dominated by the statistical error of the fit. While the slope represents the sensitivity for PbWO$_4$ monitoring, the $\chi^2$/DoF represents the linearity of the fit. It is clear that the linearity is generally good when light output loss is less than 10%. Systematic deviations exist for monitoring light of 410 and 520 nm, as compared to 440 nm, since not all wavelengths are equivalent for the monitoring.

Fig. 9 shows the monitoring sensitivity, or the slope, defined as $(\Delta T/T)/(\Delta LY/LY)$, and the linearity, defined as $\chi^2$/DoF, as a function of the monitoring wavelength for four samples. Also shown in the figure is the PMT quantum efficiency weighted radio luminescence. All these samples have a better monitoring sensitivity at shorter wavelength and the best linearity around the peak of the PMT quantum efficiency weighted radio luminescence. The better monitoring sensitivity at shorter wavelength is understood because of the poorer initial transmittance as compared to that at the longer wavelength. The best linearity around the peak of radio luminescence is caused by two radiation-induced color centers peaked at two sides of the radio luminescence with different damage and recovery speed, as discussed in detail in our previous paper [8].

Table I lists the results of our monitoring test bench for seven R&D PbWO$_4$ samples produced in China: SIC or Beijing Glass Research Institute (BGRI) and five preproduction samples produced in BTCP. Note that all are CMS full-size samples of 25 radiation lengths, or 23 cm long, with a dimension of $2.3 \times 2.3$ cm$^2$ tapered to $2.6 \times 2.6$ cm$^2$. The sample ID, the dopant in the melt, and the sensitivity and linearity at 440 and 490 nm are listed. All samples are mainly Y-doped and have similar emission spectrum peaked at 420 nm. We therefore choose 440 nm as the monitoring wavelength [8]. As discussed in our previous report [8], the 495 nm may be used as the monitoring wavelength for undoped PbWO$_4$ crystals. Since CMS uses only Y-doped PbWO$_4$ crystal, which has an

### TABLE I
MONITORING TEST-BENCH RESULT

| Sample ID | Dopant | Sensitivity ($\frac{\Delta T}{T}/\frac{\Delta LY}{LY}$) | | Linearity ($\chi^2$/DoF) | |
|---|---|---|---|---|---|
| | | 440 nm | 490 nm | 440 nm | 490 nm |
| SIC-S301 | Y/Sb | $0.43 \pm 0.01$ | $0.35 \pm 0.01$ | 1.17 | 1.59 |
| SIC-S347 | Y/Sb | $0.60 \pm 0.01$ | $0.55 \pm 0.01$ | 0.63 | 0.99 |
| SIC-S392 | Y | $0.51 \pm 0.01$ | $0.44 \pm 0.01$ | 0.94 | 1.11 |
| SIC-S412 | Y | $0.59 \pm 0.03$ | $0.49 \pm 0.03$ | 0.58 | 1.26 |
| SIC-S762 | Y | $0.51 \pm 0.01$ | $0.48 \pm 0.01$ | 0.92 | 1.14 |
| BGRI-824 | Y | $0.49 \pm 0.01$ | $0.49 \pm 0.01$ | 0.42 | 0.76 |
| BGRI-826 | Y | $0.42 \pm 0.01$ | $0.42 \pm 0.01$ | 0.71 | 0.96 |
| BTCP-2133 | Y/Nb | $0.34 \pm 0.01$ | $0.31 \pm 0.01$ | 0.45 | 0.87 |
| BTCP-2162 | Y/Nb | $0.28 \pm 0.01$ | $0.25 \pm 0.01$ | 0.62 | 1.29 |
| BTCP-5615 | Y/Nb | $0.33 \pm 0.01$ | $0.30 \pm 0.01$ | 0.78 | 1.42 |
| BTCP-5618 | Y/Nb | $0.29 \pm 0.01$ | $0.27 \pm 0.01$ | 0.48 | 0.92 |
| BTCP-5658 | Y/Nb | $0.32 \pm 0.01$ | $0.32 \pm 0.01$ | 1.04 | 2.68 |



Fig. 10.   Photo of Quantronix laser system installed at Caltech.
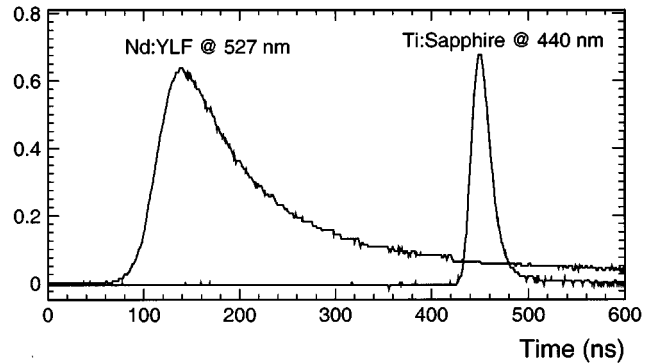


Fig. 11.   The monitoring laser pulse shape for the YLF:Nd pumping laser at 527 nm and the Ti:Sapphire laser at 440 nm.
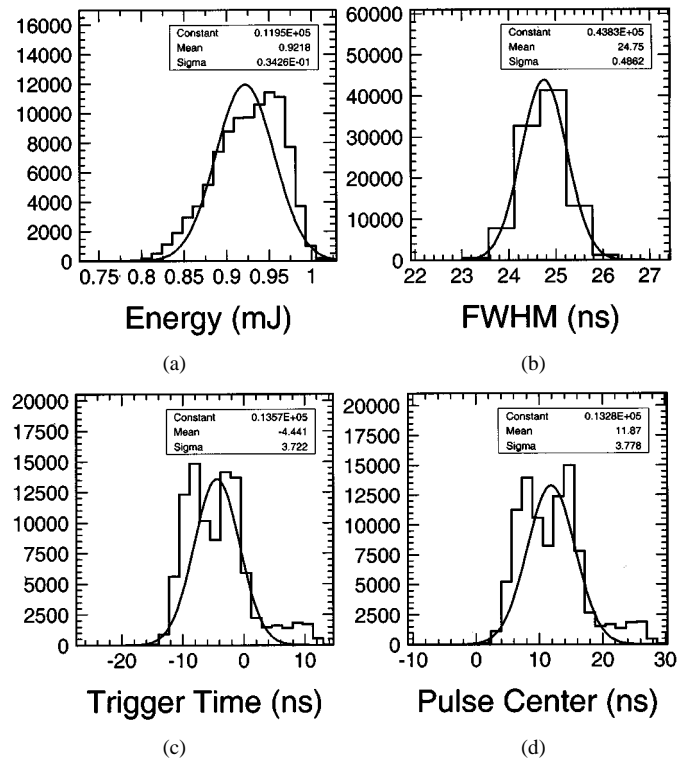


Fig. 12.   Distributions of (a) pulse energy, (b) FWHM, (c) trigger time, and (d) pulse center from monitoring Ti:Sapphire laser at 440 nm, obtained in a test run of 135 h.

emission peaked at 420 nm, this wavelength is now used as a cross-check wavelength.

## IV. LASER PERFORMANCE

The first laser system was manufactured at Quantronix Inc.[1] in 1999 and was delivered to Caltech at the end of 1999. Fig. 10 shows a photo of the laser system installed at Caltech. Fig. 11 shows laser pulse shape as recorded by a digital scope. One notices that while the pumping laser pulse is wide and has a tail, the monitoring laser pulse from the Ti:Sapphire laser at 440 nm has a clean shape and is without tail.

After initial installation and tuning, a 135-h long-term stability test was carried out when the laser was run at 440 nm at close to the maximum power. Fig. 12 shows distributions of (a) the pulse energy, (b) the FWHM, (c) the trigger time, which is defined as the half-height of the front edge of the laser pulse, and (d) the pulse center, which is defined at the intensity weighted pulse timing. The instability of the pulse energy and FWHM is found to be 3.7 and 2.0%, respectively. The jitters of both the trigger time and the pulse center are found to be 3.7 ns.

It is known that the long-term stability is usually worse than the short-term performance. We also plot the history of the pulse energy, the FWHM, and the trigger time in Figs. 13–15, respectively, where (a) the mean value in each hour and (b) the standard deviation of the distribution in each hour are plotted. As seen from these figures, the short-term stability of the pulse energy and the FWHM are 2.0 and 1.6% respectively, and the jitter of the trigger time is 1.6 ns. The pulse center has an identical distribution as the trigger time, and so is not plotted. We are pleased with the stability of the Quantronix laser system, which is much better than our 10% requirement.

By using a high-resolution monochromator (Oriel MS257) the laser spectrum was measured, and the contamination is found to be less than $10^{-3}$. Fig. 16 shows the laser pulse spectrum at 440 nm as a function of wavelength. There is no contamination between 300 and 1200 nm. The lifetime of a dc krypton lamp was found to be up to 2000 h. Typical
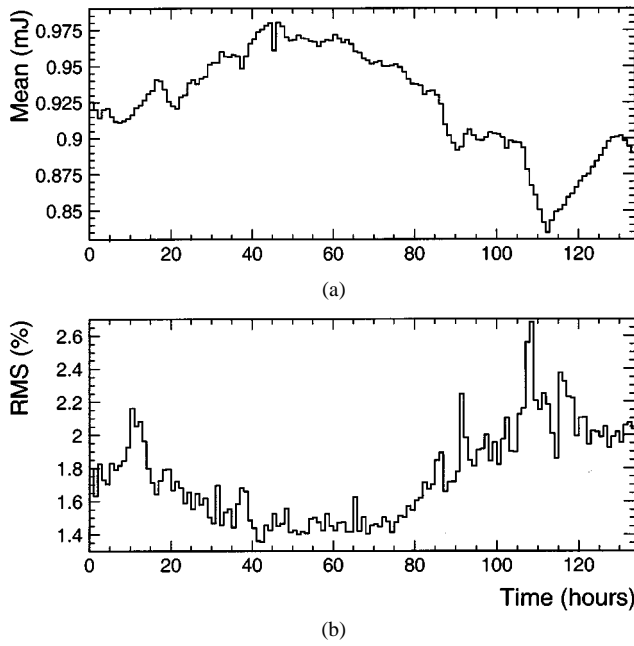
[1]Quantronix, East Setauket, NY.

Fig. 13. The history of (a) Ti:Sapphire laser pulse energy at 440 nm and (b) its standard deviation, obtained in a test run of 135 h.
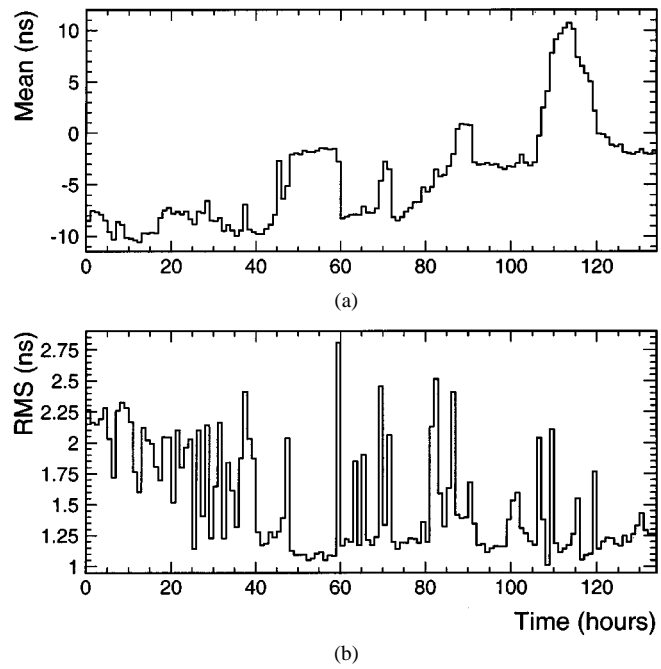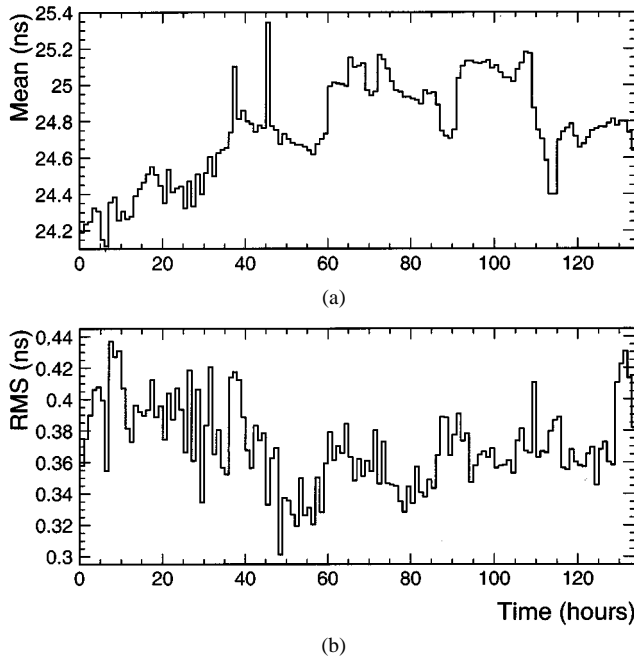


Fig. 14. The history of (a) Ti:Sapphire laser pulse width at 440 nm and (b) its standard deviation, obtained in a test run of 135 h.

power degradation is about 10 and 20% at 1000 and 2000 h, respectively.

## V. DISCUSSIONS

For intercalibration of 83 000 PbWO$_4$ crystals *in situ* at LHC, it is important to understand the consistency of the mass-produced crystals. Not only the amplitude of variations of the transmittance but also the slope, or the sensitivity, plays an important role. Since it will be difficult to measure the slope for each crystals *in situ* at LHC, or even at the test beam, one has two choices: either using a unified slope for all crystals (at least for crystals



Fig. 15. The history of (a) Ti:Sapphire laser trigger timing at 440 nm and (b) its standard deviation, obtained in a test run of 135 h.
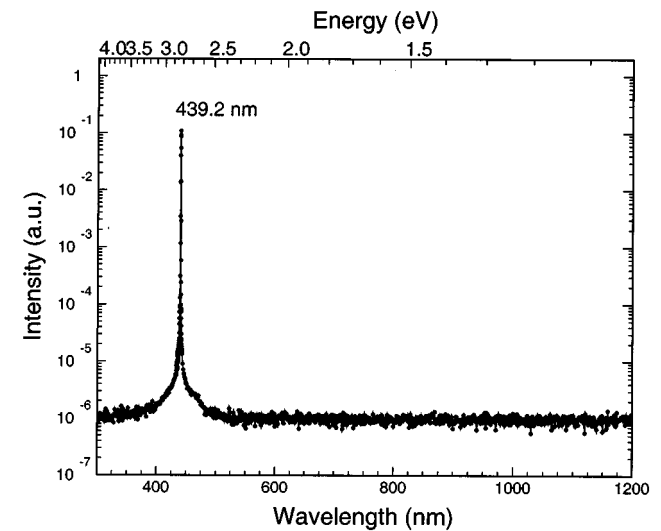


Fig. 16. Ti:Sapphire laser pulse spectrum at 440 nm is shown as a function of wavelength.

grown by the same technology) or trying to fit the absolute calibration constant and the slope at the same time by using a constraint fit to physics data, such as $Z \rightarrow e^+e^-$ [12]. The entire task would be less time-consuming if crystals were consistent. This consistency, however, requires rigorous quality control on crystal growth, including raw materials and growth parameters, since the slope is related not only to the initial transmittance, i.e., permanent absorption, but also to the radiation-induced color centers. It thus depends on the density of impurities and defects in the crystals. A particular difficulty exists for crystals grown by the Czochralski method since the raw material in one crucible is used for several poolings for economical reason, so that crystals grown in the first pooling are by definition different from that grown in the last pooling.
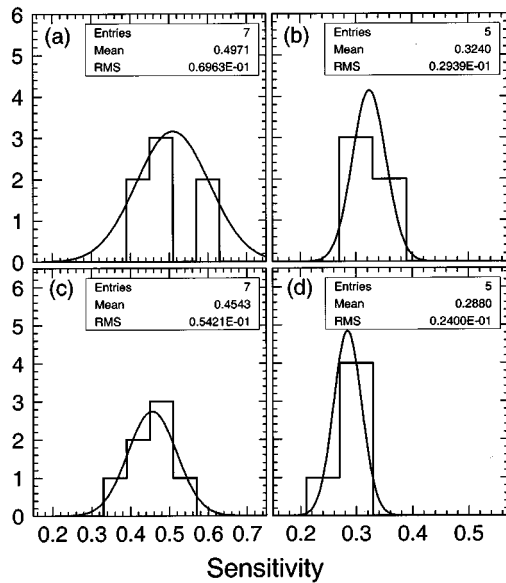
Fig. 17. Sensitivity at 440 and 490 nm is shown for the samples grown by (a) and (c) Bridgman and (b) and (d) Czochralski method, respectively.

We looked at the distribution of the slope with a limited statistics. Fig. 17 shows distribution of the sensitivity for seven samples grown by the Bridgman method in China and five samples grown by the Czochralski method in Russia. We found that the average slope is 0.50 and 0.45 at 440 and 490 nm, respectively, for samples grown by Bridgman method, and 0.32 and 0.29, respectively, for samples grown by Czochralski method. The corresponding standard deviation of the distributions is 14 and 12% at 440 and 490 nm, respectively, for samples grown by Bridgman method, and 9.1 and 8.3% for samples grown by the Czochralski method. The wider distribution of the Bridgman crystals is expected since they are R&D samples grown in two different institutions with variations of growth parameters as well as raw materials. The consistency of the Bridgman crystals is expected to be improved when all growth parameters are fixed in the preproduction stage. The 9.1% distribution obtained from five Czochralski crystals, however, indicates the difficulty to use a unified slope even for preproduction crystals.

## VI. SUMMARY

We have designed a monitoring light source and high-level distribution system to be used to provide crucial intercalibration *in situ* at LHC for a CMS PbWO$_4$ crystal calorimeter. The system is capable of providing monitoring light pulses at monitoring wavelength of choice up to 10 kHz with dynamic range reach up to 1.3 TeV and running continuously with 100% efficiency during data-taking.

A key issue of wavelength choice was resolved by a monitoring test bench. Seven Y-doped R&D PbWO$_4$ samples grown by the Bridgman method in China and five Y/Nb-double-doped preproduction samples grown by the Czochralski method in Russia were measured. Consistent sensitivity and linearity were found for crystals grown by the same technology. The better sensitivity at UV is understood to be caused by lower transmittance, and the best linearity around emission peak is

understood to be caused by two color centers peaked at two sides of emission and with different damage and recovery speed. To achieve the best linearity and adequate sensitivity, 440 nm is chosen as the monitoring wavelength.

A 135-h long-term stability test was carried out for the monitoring laser system. The result of the test shows that the laser system provides pulse energy of 1.0/0.6 mJ and FWHM of 25/35 ns at 440/500 nm. The long-/short-term stability for pulse energy and width are 3.7/2.0% and 2.0/1.6%, respectively. The long- and short-term jitter are found to be 3.7 and 1.6 ns, respectively. The system also provides clean laser spectral output with contamination of less than $10^{-3}$.

With limited statistics, the consistency of the slope, or sensitivity, was studied, and was found to be 14 and 9.1%, respectively, for seven R&D samples grown by the Bridgman method and five preproduction samples grown by Czochralski method. While the poor consistency of Bridgman R&D samples is attributed to the variations of growth parameters during the R&D phase, the 9.1% distribution of the Czochralski preproduction samples indicates the difficulty of using a unified slope parameter for all crystals *in situ* at LHC.

## REFERENCES

[1] H. F. Chen, K. Deiters, H. Hofer, P. Lecomte, and F. Nessi-Tedaldi, "Radiation damage measurements of undoped lead tungstate crystals for the CMS electromagnetic calorimeter at LHC," *Nucl. Instrum. Meth.*, vol. A414, pp. 149–155, 1998.
[2] P. Lecoq, I. Dafinei, E. Auffray, M. Schneegans, M. Korzhik, and V. Pavlenko *et al.*, "Lead tungsten scintillators for LHC EM calorimetry," *Nucl. Instrum. Meth.*, vol. A365, pp. 291–298, 1995.
[3] M. Kobayashi, M. Ishii, and Y. Usuki, "Comparison of radiation damages of different PbWO$_4$ scintillating crystals," *Nucl. Instrum. Meth.*, vol. A406, pp. 442–450, 1998.
[4] A. Annenkov, V. Ligun, E. Auffray, P. Lecoq, A. Borisevich, and M. Korzhik, "Suppression of the radiation damage in lead tungstate scintillation crystal," *Nucl. Instrum. Meth.*, vol. A426, pp. 486–490, 1999.
[5] M. Nikl, P. Bohacek, E. Mihokova, S. Baccaro, A. Vedda, and M. Diemoz *et al.*, "Radiation damage processes in wide-gap scintillating crystals: New scintillation materials," *Nucl. Phys. Proc. Suppl.*, vol. 78, pp. 471–478, 1999.
[6] R. Y. Zhu, Q. Deng, H. Newman, C. Woody, J. Kierstead, and S. Stoll, "A study on the radiation hardness of lead tungstate crystals," *IEEE Trans. Nucl. Sci.*, vol. 45, pp. 686–691, June 1998.
[7] R.-Y. Zhu, "Radiation damage in scintillating crystals," *Nucl. Instrum. Meth.*, vol. A413, pp. 297–311, 1998.
[8] X. Qu, L. Zhang, and R.-Y. Zhu, "Radiation induced color centers and light monitoring for lead tungstate crystals," IEEE Trans. Nucl. Sci., to be published.
[9] "The Electromagnetic Calorimeter Technical Design Report," CMS Collaboration, CERN/LHCC 97-33, 1997.
[10] "The LHC Conceptual Design Report," The LHC Study Group, CERN/AC/95-05 46, 1995.
[11] L. Zhang, R.-Y. Zhu, and D. Liu, "Monitoring Lasers for PbWO$_4$ ECAL,", CMS Internal Note 1999/014, 1999.
[12] R.-Y. Zhu, "On quality requirements to the barium fluoride crystals," *Nucl. Instrum. Meth.*, vol. A340, pp. 442–457, 1994.